Multifrequency 3-D Inversion of GREATEM Data by BCGS-FFT-BIM

Chen Qiu, Bingyang Liang, Feng Han, *Member, IEEE*, Hai Liu, *Member, IEEE*, Chunhui Zhu, Na Liu, *Member, IEEE*, Fubo Liu, Guangyou Fang, and Qing Huo Liu, *Fellow, IEEE*

***Abstract*— A newly designed grounded electrical-source airborne transient electromagnetics (GREATEM) system was introduced recently. Detailed data preprocessing techniques to acquire the high-precision measured magnetic field are discussed here. Different from the previous work in which the reconstruction of the underground structure is performed in 1-D, we interpret the GREATEM data in 3-D by the volume integral equation (VIE) method in the frequency domain. Therefore, the VIE in the forward electromagnetic scattering model is formulated in the low-frequency regime. It is solved by using the stabilized biconjugate gradient fast Fourier transform (BCGS-FFT) method. In the nonlinear inversion, the Born iterative method (BIM) and the conjugate gradient method are adopted to minimize the cost function. A synthetic model of GREATEM survey is used to validate the proposed 3-D forward and inversion algorithms. Then, the field data from two GREATEM surveys are used to test the effectiveness and accuracy of the proposed inversion algorithm. The reconstructed conductivity structures are consistent with geological drilling results, confirming the potential of our method for solving the 3-D GREATEM inversion problems in geophysical engineering applications. This paper represents the first application of the BCGS-FFT and BIM algorithms to a GREATEM system.**

***Index Terms*— Born iterative method (BIM), grounded electrical-source airborne transient electromagnetics (GREATEM), stabilized biconjugate gradient fast Fourier transform (BCGS-FFT), volume integral equation (VIE).**

I. Introduction

THE airborne transient electromagnetics (TEM) is a widely used technique to survey the geological properties of a large or inaccessible underground region. In the last few decades, airborne TEM has made a remarkable progress in engineering applications, such as groundwater detection, mineral exploration, and so on [1]–[3]. However, the penetration depth of airborne TEM is usually limited to about hundreds of meters [4] due to the short distance between the transmitter and the receiver. To increase the penetration depth, a new semiairborne electromagnetic (EM) system called the grounded electrical-source airborne transient electromagnetic (GREATEM), which is first proposed by Mogi *et al.* [5], has been developed and improved in survey applications [6]–[8]. The GREATEM system uses an airborne receiver hang but a grounded electrical line source as the transmitter. With the grounded source, the system can produce a larger source moment to obtain a greater depth of investigation. Although the survey area is limited by this experimental setting, the GREATEM system still shows the advantages over conventional airborne TEM systems. By using a helicopter, the GREATEM system is useful for surveying the steep slope mountainous area in a safety way. The coastal area surveying is also benefited from the GREATEM systems due to the experimental towed magnetic receiver in the air for environmental issues. Other advantages, such as the moderate signal-to-noise ratio (SNR), are also obvious in the GREATEM system compared with other TEM measurements.

The airborne TEM survey always generates a large amount of data for reconstructing the underground region. Therefore, the interpretation of airborne TEM data is mostly achieved in 1-D, because the transmitter and receiver move together along the flight path, and it is fast and has low computation costs. However, reconstructed structures of these 1-D airborne TEM inversion methods have shown discontinuities [9]. Thus, it is difficult to reconstruct a reasonable result for complex earth structures by using a 1-D inversion method, especially in GREATEM. In recent years, the 3-D inversion attracts more interest in airborne TEM data processing. There are several algorithms for airborne TEM data interpretation in which the forward computation is performed in the time domain. Wang *et al.* [10] employed the finite-difference time-domain (FDTD) method for the backpropagation in 3-D inversion used in crosswell TEM surveys. Haber *et al.* [11] developed the finite-volume method for 3-D EM inversion in the time-domain modeling. It is also feasible to use the inverse Fourier transform of the frequency-domain response to obtain the time-domain solution. Sugeng [12] applied the finite-element method to simulate TEM response for 3-D complex geological structure efficiently. Wilson *et al.* [13] introduced an inversion algorithm based on the Gauss–Newton method to invert airborne EM data in 2.5-D modeling geoelectrical

Manuscript received March 2, 2018; revised June 24, 2018 and July 27, 2018; accepted September 27, 2018. Date of publication October 24, 2018; date of current version March 25, 2019. This work was supported in part by the National Natural Science Foundation of China under Grant 4150411 and Grant 41504120 and in part by the Special Program for Applied Research on Super Computation of the NSFC-Guangdong Joint Fund (the second phase) under Grant U1501501. *(Corresponding authors: Feng Han; Qing Huo Liu.)*

C. Qiu, B. Liang, F. Han, C. Zhu, and N. Liu are with the Department of Electronic Science, Institute of Electromagnetics and Acoustics, Xiamen University, Xiamen 361005, China (e-mail: feng.han@xmu.edu.cn).

H. Liu is with the School of Civil Engineering, Guangzhou University, Guangzhou 510006, China.

F. Liu and G. Fang are with the Institute of Electronics, Chinese Academy of Sciences, Beijing 100190, China.

Q. H. Liu is with the Department of Electrical and Computer Engineering, Duke University, Durham, NC 27708 USA (e-mail: qhliu@duke.edu).

Color versions of one or more of the figures in this paper are available online at http://ieeexplore.ieee.org.

Digital Object Identifier 10.1109/TGRS.2018.2873363

cross section. Abubakar *et al.* [14] and Cox *et al.* [15] used the integral equation method for EM forward modeling for the inversion of 3-D conductivity structure in airborne TEM surveys.

On the other hand, most inversion of the GREATEM data is performed in the time domain and in 1-D, although the forward EM response can be computed in either time domain or frequency domain. Only the later time response data are exploited [6], [16] to avoid the early influence of the current source. Ito *et al.* [3] applied the 1-D staggered finite-difference approximation to calculate the forward EM response in the frequency domain. Then, the transient response in the time domain is obtained by the inverse Fourier transform and compared with the measured transient field at receivers to invert to the resistivity structure. Ito *et al.* [7] and Allah *et al.* [16] later extended this paper to 3-D to explain the experimental data in the coastal area, which overcomes the sea effect problem in 1-D inversion.

In our previous work, the 1-D inversion of GREATEM measurement [17] has been proven to be effective. In this paper, we present a frequency-domain 3-D inversion algorithm for the reconstruction of the anomaly buried in a layered medium from the GREATEM measurement. The 3-D forward EM scattering model is formulated by the volume integral equation (VIE) in the layered media. Although the conventional method to solve the VIE is the method of moment (MOM), it is not frequently adopted in engineering applications due to the high computation resource consumption.

Iterative methods, such as conjugate gradient (CG) [18] and biconjugate gradient [19], are preferred. The stabilized biconjugate gradient (BCGS) method [20] is another fast solver that has been used to solve VIE. Due to the shift invariance of the layered medium dyadic Green's function, fast Fourier transform (FFT) is used to accelerate the BCGS iteration and it has made a great success for solving the VIEs in the layered media. Millard and Liu [21] have used the stabilized biconjugate gradient fast Fourier transform (BCGS-FFT) method to solve the large-scale scattering problems, and it shows a significant improvement in efficiency over the MOM or other CG-type methods. In the nonlinear inverse problem, the conductivity profile of the buried anomaly is solved iteratively through minimizing the misfit between the measured and the calculated scattered field. Several algorithms for the inversion have been proposed, such as the contrast source inversion method [22], Born iterative method (BIM) [23], and distorted BIM (DBIM) [24].

Numerical simulations show that the DBIM converges faster than the BIM, while the BIM is more tolerant to noise than DBIM. In addition, the layered medium Green's function of the background does not need to be updated for the BIM [24]. Therefore, we adopt the BIM algorithm to reconstruct the buried scatterer for the GREATEM measurement.

This paper is organized as follows. The GREATEM system and data preprocessing are introduced in Section II. In Section III, the EM forward scattering model is established in the form of VIE for the GREATEM measurement. The BCGS-FFT and the BIM algorithm are briefly described, and the 3-D inversion method is introduced. Synthetic data are first used to validate the forward modeling and inverse algorithm in Section IV. In Section V, we use the field data from our recent GREATEM experiments to test the inversion algorithm. The summary and conclusion are given in Section VI.

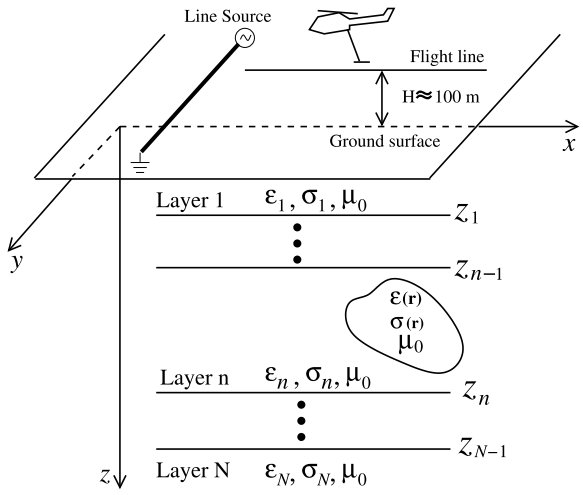

Fig. 1. Geometry for GREATEM survey with the anomaly buried in a layered medium.

II. Survey Method

A. GREATEM System

A GREATEM system usually uses a 2∼3 km grounded electrical line source as the transmitter and a three-component magnetometer as the receiver to measure the magnetic field in a towed bird suspended by a rope under the helicopter. The transmitter current of the GREATEM is usually a bipolar square waveform. The data of GREATEM survey system recorded in the time domain provide a full-wave time series of the magnetic field induced by the eddy current in the ground after the transmitting current is cut off. The whole system is synchronized with the high-precision clock installed in the helicopter. The GREATEM system shows advanced features by combining the grounded and airborne systems. For example, the data recorded in the GREATEM system have intermediate SNR and cost of logistics between the grounded and airborne systems [4].

In this paper, we report a new GREATEM system designed by the Institute of Electronics, Chinese Academy of Sciences. The line source is placed on the ground, as shown in Fig. 1. The helicopter has a global position system (GPS) and a high-accuracy gyro sensor attached in the towed bird. The GPS system provides the coordinates of detector and synchronizes the whole experimental system. The data acquisition system consists of a 16-bit analog-to-digital converter at a sampling rate of 48 kHz, which is installed on the helicopter with the same GPS system. Due to the limited band of the system electronics, the current of the transmitter is not an ideal bipolar square waveform but a bipolar trapezoidal waveform with a 20-A amplitude and the 50% duty cycle, as shown in Fig. 2. The waveform has a periodic form of $-I, 0, +I, 0$; each ON/OFF time interval is 0.02 s, and thus, the period of the waveform is 0.08 s. The triaxis receiver is composed of three orthogonal magnetic coils. Each coil has an effective

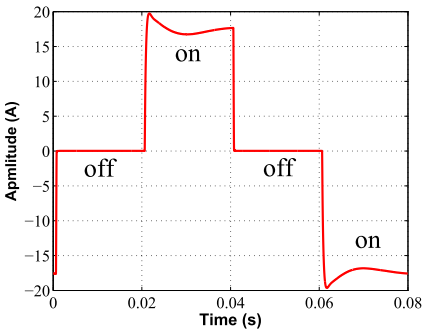

Fig. 2. One period of the waveform of source current employed by the GREATEM system.

area of 580 m^2. The directions of the triaxis receiver are recorded by the gyro installed in the helicopter. The raw data recorded by the following data acquisition system are voltage signals.

B. Data Preprocessing

To obtain high-quality data with an acceptable SNR, a series of data processing techniques is applied to the experimental data before interpretation. The processing procedure includes the removal of slow-varying component, attitude correction, data stacking of the raw data, and magnetic field spectrum computation. In the following, we will describe these four steps in detail.

1) *Removal of Slow-Varying Component:* The raw data of the GREATEM measurement always have the slow-varying component [17]. Therefore, before performing the inversion, we at first extract the direct component (dc) by computing the arithmetic mean value of each period raw data. Then, we subtract this dc component from the raw data for each period. In this stage, the signals still contain slow-varying component although the dc component has been removed. In each period, there are four rising edges (included in both the positive and negative pulses). As described in [17], we pick four data values before each rising edge and fit them with a quadratic curve. The curve signal is treated as the slow-varying component and removed by subtracting it from the GREATEM data. Fig. 3(a) shows the comparison between the raw data and those after the removal of slow-varying component in a time window of 1 ms to enlarge the system response to the negative falling edge of the source current.
2) *Attitude Correction:* During data collection of the GREATEM survey flight, the receiver coil has three types of motions, namely, the roll, pitch, and yaw rotations [25]. Therefore, a geometry correction is needed, because the movements of receivers lead to the deviation of local coordinate of the three orthogonal magnetic sensors away from the global coordinate defined in the measurement. The roll, pitch, and yaw rotations are detected and the posture data are recorded by the gyro attached to the towed bird. The attitude corrections are made using the triaxis orthogonal coordinate transformation described in [25]. The posture of the receiver is recorded in every transmission cycle, and thus, the attitude correction is made for every transmission cycle.

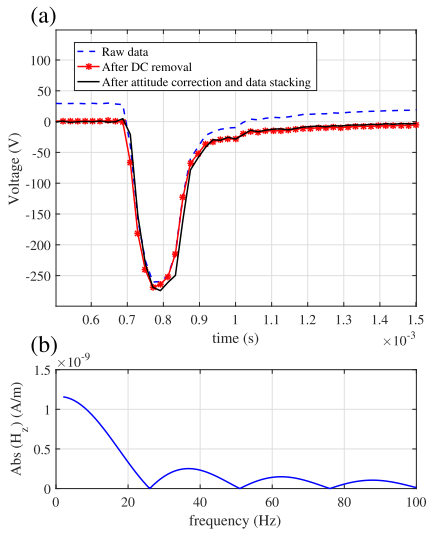

Fig. 3. Example of voltage signals in the GREATEM system for four steps of data preprocessing. (a) Different voltage signals at the receiver for each data processing step. The signals in only a time window of 1 ms are shown. (b) Measured total magnetic field H_z spectrum in the GREATEM.

3) *Data Stacking:* To suppress the random noise, data stacking in the time domain is necessary for GREATEM systems. Since the helicopter is designed to move at a speed of 54 km/h, we use 50 transmission cycles (around 60-m covering distance) to stack the transient signals. The stacking number can be reduced if a higher SNR is available. The transient signal after stacking is treated as the measured data at the middle point of the covering distance. In the practical measurement, the movement of the helicopter is affected by wind. Therefore, the covering distance of data stacking is not exactly 60 m. Fortunately, the location of the receiver in every transmission cycle is recorded by the GPS system. In order to perform the FFT in our BCGS-BIM algorithm, we conduct a 2-D linear interpolation to obtain the uniformly distributed measurement point data from the stacking data. The transient signal after attitude correction and stacking is shown in Fig. 3(a).
4) *Magnetic Field Spectrum Computation:* The voltage signals after stacking are transformed into frequency domain using discrete Fourier transform. Finally, the magnetic field spectrum is calculated through dividing the voltage's spectrum by the effective coil area. The magnetic spectrum is shown in Fig. 3(b).

The data preprocessing procedure does not take too much time. Tests show that all the above-mentioned four steps together take less than 1 min in a computer with the CPU of 2.7 GHz for one flight line with a 2-km length. It is obvious that the procedure for each flight line is independent, and therefore, we can perform the preprocessing for all flight lines at the same time.

III. 3-D Forward Modeling and Inversion Methodology for GREATEM

The brief description of a forward EM scattering model and inverse algorithm for the GREATEM experimental system is given in this section.

A. Forward Modeling of GREATEM

As shown in Fig. 1, the GREATEM survey system is positioned on the top of an N-layer background medium that extends to infinity in the x- and y-directions. The properties of each layer are characterized by permittivity ϵ_n, conductivity σ_n, and permeability μ_0. In the nth layer, the total electric field $\mathbf{E}_n^{\text{tot}}$, scattered electric field $\mathbf{E}_n^{\text{sct}}$, and incident field $\mathbf{E}_n^{\text{inc}}$ satisfy the relationship

$$\mathbf{E}_n^{\text{inc}} = \mathbf{E}_n^{\text{tot}} - \mathbf{E}_n^{\text{sct}} \tag{1}$$

where $\mathbf{E}_n^{\text{tot}}$ and $\mathbf{E}_n^{\text{inc}}$ are the electric field with and without the scattering object, respectively. In the GREATEM data interpretation, the data in the low-frequency range from several hertz to several hundreds of hertz are used. Therefore, the EM wave behaves like a diffusive field. The complex permittivity and the wavenumber of the ith layer can be simplified as $\tilde{\epsilon}_i = \epsilon_i - j\sigma_i/\omega \approx -j\sigma_i/\omega$ and $k_i = \omega(\tilde{\epsilon}_i\mu_0)^{1/2} \approx \omega(-j\sigma_i\mu_0/\omega)^{1/2}$, respectively. The scattered electric field $\mathbf{E}_i^{\text{sct}}$ in the ith layer can be expressed in terms of the magnetic vector potential as

$$\mathbf{E}_i^{\text{sct}} = -j\omega\mathbf{A}_{\text{in}}(\mathbf{r}) + \frac{1}{\sigma_i\mu_0}\nabla\nabla\cdot\mathbf{A}_{\text{in}}(\mathbf{r}) \tag{2}$$

where $\mathbf{A}_{\text{in}}(\mathbf{r})$ denotes the magnetic vector potential in the ith layer due to the induced current source inside the scattering object in the nth layer.

In the layered medium, the magnetic vector potential $\mathbf{A}_{\text{in}}(\mathbf{r})$ can be calculated by

$$\mathbf{A}_{\text{in}}(\mathbf{r}) = j\omega\mu_0\int_V \mathbf{G}_{\text{in}}^{\text{AJ}}(\mathbf{r},\mathbf{r}')\cdot\chi(\mathbf{r}')\mathbf{D}(\mathbf{r}')d\mathbf{r}' \tag{3}$$

where V is the volume of object, $\mathbf{D}(\mathbf{r}) \approx -j\sigma_i\mathbf{E}(\mathbf{r})/\omega$ is the electric flux density, and $\mathbf{G}_{\text{in}}^{\text{AJ}}$ is magnetic vector potential dyadic Green's function of the layered medium. The details of the derivation of $\mathbf{G}_{\text{in}}^{\text{AJ}}$ is given in [26]. In (3), χ is the contrast function and is defined

$$\chi(\mathbf{r}) \approx \frac{\sigma(\mathbf{r}) - \sigma_n}{\sigma(\mathbf{r})}. \tag{4}$$

Substituting (2) and (3) into (1), we can obtain the electric-field integral equation (EFIE) [27] for the GREATEM measurement

$$\mathbf{E}_n^{\text{inc}}(\mathbf{r}) = -\frac{\omega}{\sigma_n}\mathbf{D}_n(\mathbf{r}) + (j\omega\sigma_n\mu_0 - \nabla\nabla\cdot) \times\int_V \mathbf{G}_{\text{in}}^{\text{AJ}}(\mathbf{r},\mathbf{r}')\cdot\chi(\mathbf{r}')\mathbf{D}_i(\mathbf{r}')d\mathbf{r}'. \tag{5}$$

When (5) is solved, it is convenient to let $i = n$ and $\mathbf{r} \in V$ [28]. In this way, (5) can be compactly rewritten as

$$\mathcal{L}[\mathbf{D}_n(\mathbf{r})] = \mathbf{E}_n^{\text{inc}}(\mathbf{r}) \tag{6}$$

where $\mathcal{L}$ is a linear operator and $\mathbf{D}_n$ is the unknown to be solved.

Equation (6) cannot be solved analytically. It must be discretized and solved by the BCGS iteration numerically. In addition, it is noted that the integration in (5) is convolution and correlation. Therefore, it can be accelerated by the discrete Fourier transform. The detail of a BCGS-FFT application can be found in [21]. Once the electric flux density $\mathbf{D}_n(\mathbf{r})$ inside the computation domain is obtained by the BCGS-FFT method, the scattered magnetic field $\mathbf{H}^{\text{sct}}$ at any location can be calculated by

$$\mathbf{H}^{\text{sct}}(\mathbf{r}) = \sigma_i\int_V \mathbf{G}_{\text{in}}^{\text{HJ}}(\mathbf{r},\mathbf{r}')\cdot\chi(\mathbf{r}')\mathbf{D}(\mathbf{r}')d\mathbf{r}' \tag{7}$$

where $\mathbf{G}_{\text{in}}^{\text{HJ}}(\mathbf{r},\mathbf{r}')$ is the dyadic Green function for the magnetic field in the ith layer due to an electric current source in the nth layer. The derivation of $\mathbf{G}_{\text{in}}^{\text{HJ}}$ can be found in [26].

B. Inversion

The goal of the inversion is to determine the distribution of electrical parameters of unknown scattering objects. The contrast function $\chi(\mathbf{r})$ is used for parameterizing the scattering object and solved from (7) in which the scattering magnetic field $\mathbf{H}^{\text{sct}}$ is assumed to be measured data. We can discretize (7) by the trapezoidal rule and obtain the compact form as

$$\mathbf{f} = \mathbf{M}[\chi] \tag{8}$$

where $\mathbf{f}$ denotes the measured scattered magnetic field in multiple sampling frequencies, $[\chi]$ is an N-dimensional column vector of the contrast function, and $\mathbf{M}$ is a matrix that is given by

$$\mathbf{M}(\mathbf{r}) = -\sigma_n\Delta V\mathbf{G}_{\text{in}}^{\text{HJ}}(\mathbf{r},\mathbf{r}')\cdot\mathbf{D}(\mathbf{r}'). \tag{9}$$

ΔV in (9) is the volume of the small voxel used to discretize V.

The inverse problem is nonlinear, because $\mathbf{M}$ in (9) is also a function of χ. Fortunately, the BIM can handle the nonlinear inverse problem efficiently and does not require to update the background Green's function.

In the BIM, the cost function with the Tikhonov regularization applied after the mth iteration is defined as

$$F_{m+1}(\chi) = \frac{||\mathbf{f} - \mathbf{M}_m\cdot\chi_{m+1}||^2}{||\mathbf{f}||^2} + \gamma^2\frac{||\chi_{m+1}||^2}{||\chi_m||^2} \tag{10}$$

where $||\cdot||$ denotes the L_2 norm on the inverse domain and γ^2 is the regularization parameter. The data of $\mathbf{f}$ are consisting of measured scattered magnetic field in the sequence of $\mathbf{f}(\omega_1)$, $\mathbf{f}(\omega_2)\cdots$, $\mathbf{f}(\omega_L)$, where L is the number of sampling frequencies used in the inversion. The matrix $\mathbf{M}$ is also assembled in a similar way by $\mathbf{G}^{\text{HJ}}$ and the total flux $\mathbf{D}$ evaluated for frequency $\omega_1, \omega_2, \cdots, \omega_L$. The cost function is solved by using measured data in all sampling frequencies simultaneously to exploit as more information as possible. To minimize the cost function, (10) can be solved through its equivalent form [29]

$$\left(\frac{\mathbf{M}_m^\dagger\mathbf{M}_m}{||\mathbf{f}||^2} + \frac{\gamma^2}{||\chi_m||^2}\mathbf{I}\right)\chi_{m+1} = \frac{\mathbf{M}_m^\dagger\mathbf{f}}{||\mathbf{f}||^2} \tag{11}$$

where the superscript † denotes the complex conjugate transposition. To obtain the model parameter χ_{m+1}, the CG method is applied to solve (11). The contrast function will be updated iteratively until the cost function reaches an acceptable misfit or the procedure reaches its maximum iteration number. The regularization parameter γ is used to maintain the iteration stability in this ill-posed problems. However, a larger γ value will cause larger errors in the inversed χ. The method to choose the value of γ can be referred to [30].

C. Extraction of the Scattered Magnetic Field

As we discussed earlier, the measured scattered magnetic field is needed in the inversion. However, only the total magnetic field is measured in the GREATEM experiment. Therefore, we will discuss how to extract the scattered field response from the total magnetic field. Similar to the electric field relationship discussed in (1), the scattered magnetic field is also equal to the total magnetic field subtracted by the incident magnetic field. The incident magnetic field $\mathbf{H}^{\text{inc}}$ in a multilayered medium is the field at the receiver when the scatterer is absent. The spectrum of $\mathbf{H}^{\text{inc}}$ at any location $\mathbf{r}$ can be expressed as

$$\mathbf{H}^{\text{inc}}(\mathbf{r}) = \int \mathbf{G}^{\text{HJ}}(\mathbf{r}, \mathbf{r}') \cdot \mathbf{J}(\mathbf{r}') d\mathbf{r}' \tag{12}$$

where $\mathbf{J}(\mathbf{r}')$ is the spectrum of the current source and is known in the GREATEM measurement. However, the Green's function $\mathbf{G}^{\text{HJ}}$ depends on the conductivity of the layered background that is sometimes unknown. Therefore, before inversion, we will first try to collect the geological drilling data to infer the background conductivity information. After $\mathbf{H}^{\text{inc}}$ is calculated, the scattered magnetic field can be obtained by subtracting the incident field from the total field. In the worst case, if there is no *a priori* information of the survey area, we perform the inversions by using different background conductivity values. The reconstructed underground profile is chosen as the most reliable result when the data misfit is the smallest. Numerical experiments show that the reconstructed conductivity of the buried anomaly is sensitive to the background parameter, and a 5% deviation of the background conductivity will cause 17.5% error of the reconstructed result.

D. Inversion Scheme

The flowchart of the 3-D EM inversion algorithm for GREATEM data is shown in Fig. 4, and it mainly consists of eight steps.

1) Preprocess the GREATEM data to obtain the three components of the total magnetic transient response.
2) Transform the total measurement response into the frequency domain and extract the scattered magnetic field.
3) Obtain the background conductivity σ, calculate, and store the layered background medium Green's functions.
4) Setup the initial model parameter χ, let the iteration number $m = 0$, set the threshold and maximum iteration number, and input the secondary magnetic field spectrum.
5) Solve the discretized 3-D forward VIE by using the BCGS-FFT and obtain the scattered magnetic field $\mathbf{H}^{\text{sct}}$ at the receiver locations.
6) Calculate the misfit between the extracted scattered field and the calculated field. If the misfit is smaller than the prescribed threshold or the iteration number reaches the maximum user-defined number, exit the inversion iteration; otherwise, continue.
7) Minimize the cost function and obtain the updated contrast $\chi_{m+1}(\mathbf{r})$.
8) Set the iteration number $m = m+1$ and return to step 5.

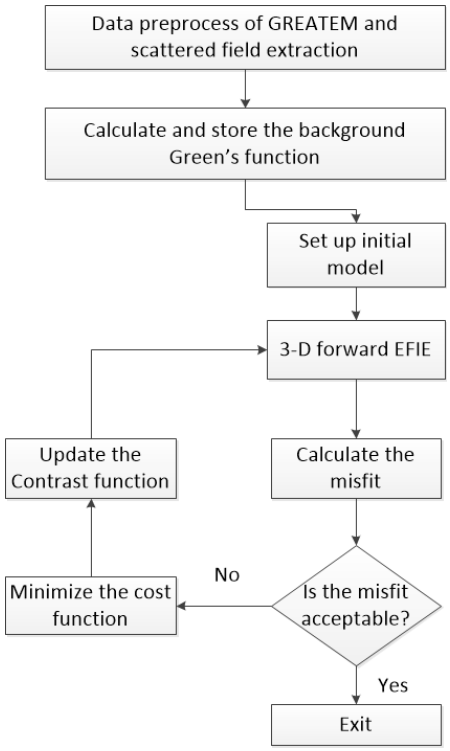

Fig. 4. Flowchart of the 3-D inversion algorithm for GREATEM measurement.

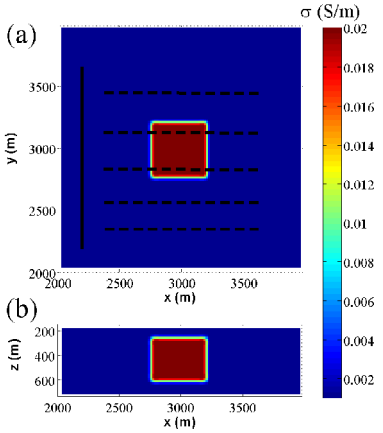

Fig. 5. Model scheme used to generate synthetic data for validating the 3-D EM forward and inversion algorithms. (a) Horizontal slice at $z = 400$ m. The solid line denotes the line source and the dashed lines are the flight lines for GREATEM survey. The receivers are in these lines. (b) Vertical slice at $x = 2000$ m that shows the location of the scattering object.

IV. Numerical Experiment

To demonstrate and validate the proposed 3-D inversion algorithm for GREATEM data in the frequency domain, a geophysical model is first used to generate synthetic data for reconstructing the conductivity of a scattering object buried underground. We choose six frequencies 7, 10, 15, 18, 21, and 25 Hz to perform the multifrequency inversion.

We first investigate the conductivity reconstruction for the model shown in Fig. 5, which contains a cubic scatterer with the conductivity of 0.02 S/m buried in underground soil with the conductivity of 0.005 S/m. The scattering object has the size of 400 m × 400 m × 300 m with its center located

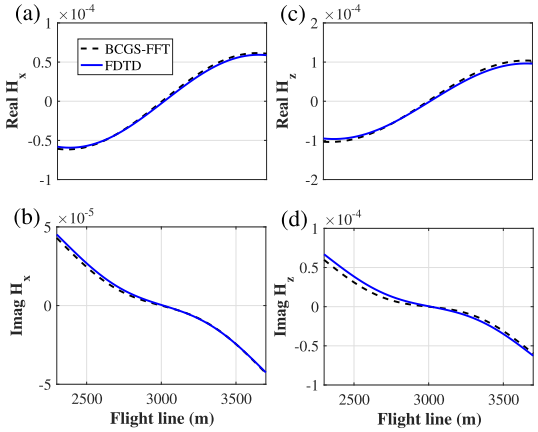

Fig. 6. Comparisons of scattered magnetic fields between FDTD simulations and BCGS-FFT iteration solution for the 3-D model in Fig. 5. (a) and (b) Real and imaginary parts of H_x component, respectively. (c) and (d) Real and imaginary parts of H_z component, respectively.

at $z = 400$ m below the ground surface. The transmitter is assumed to be a 1.5-km-long line source on the ground, and the receivers are 100 m above the ground. The total magnetic field of the synthetic data is calculated using the FDTD method. The Blackman–Harris Window function [31] is used as the excitation source in the FDTD simulation to avoid the so-called "inverse crime" where both the synthetic data and inversion use the same forward solver and discretization.

To validate the precision of the 3-D forward modeling of GREATEM, we use the BCGS-FFT algorithm to compute the scattered field at the receiver array in the dashed lines shown in Fig. 5. The scattered magnetic fields in one flight line computed by our BCGS-FFT forward solver are shown in Fig. 6 and agree well with the FDTD simulation results. The relative error of scattering field between BCGS-FFT and FDTD is 4.29% if we treat the FDTD simulated result as a reference. Here, we only compare the x- and z-components of the scattered magnetic fields and omit the y-component, since the line source is along the y-direction. The computational time of BCGS-FFT only takes a few minutes for one frequency, but the FDTD's full-wave simulation needs several hours. Therefore, our 3-D forward modeling of the GREATEM is accurate and fast for the large-scale inversion.

In the following, let us verify our inversion algorithm. The background model is set to be a half-space configuration with the underground soil conductivity of 0.005 S/m. The computation domain is 2 km × 2 km × 0.8 km and is divided into 50×50×20 cells with the grid size of 40 m. The maximum magnitude of the synthetic scattered magnetic field data for all frequencies is contaminated with 10-dB random white Gaussian noise. The inversion is performed on a cluster work station with 20-cores Xeon E2650 v3 2.3 GHz CPU, 512 GB RAM. The misfit between the calculated and the measured data is stable at 6.14% after 11 iterations, and the total computational time is 2.38 h. Fig. 7 shows the reconstructed 3-D conductivity distribution of the buried object. It is clear that both the location and the shape of the scattering object can be identified. The inverted conductivity of the object is

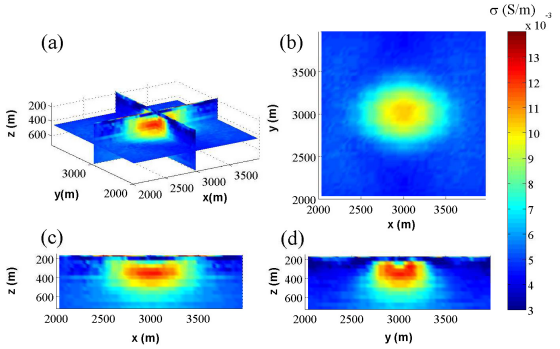

Fig. 7. Reconstructed conductivity from synthetic data for the model in Fig. 5. (a) 3-D slices of the inverted results. (b) Horizontal slice through the center of the object at $z = 400$ m. (c) Vertical slice through the center of the object at $y = 3000$ m. (d) Vertical slice through the center of the object at $x = 3000$ m.

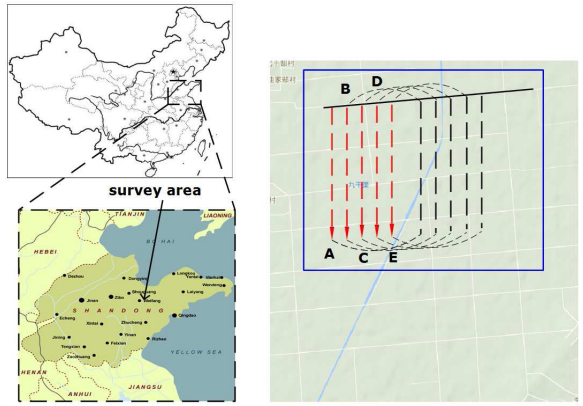

Fig. 8. Location and geometry for the GREATEM experimental survey conducted in Shandong, China. The solid line indicates the transmitter cable (electrical line source), which is placed along the road with the length of 2.768 km. The dashed lines (A–E) are the flight lines.

0.0173 S/m, which is close to the true value. Both the location and conductivity of the object can be well reconstructed by our inversion algorithm.

To quantitatively evaluate the model misfit of the reconstructed conductivity profile, we define the mean square error (MSE) and $\mathrm{Err}_{\max}$ according to [32] as

$$\mathrm{MSE} = \frac{\|\chi^t - \chi^r\|^2}{\|\chi^t\|^2} \tag{13}$$

and

$$\mathrm{Err}_{\max} = \frac{\|\chi^t\|_\infty - \|\chi^r\|_\infty}{\|\chi^t\|_\infty} \tag{14}$$

where the superscript t means the true value, r denotes the reconstructed values, and $||\cdot||_\infty$ is the uniform norm. In this numerical experiment, the MSE is 13.4% and $\mathrm{Err}_{\max}$ is 13.5%.

V. Field Experiments

In January 2016, a GREATEM survey was conducted in Shandong, China. The survey region includes several explored mines and some are still being explored. As shown in Fig. 8, the electric line source is placed along the road from the west to the east. The source current moment is 20 A × 2768 m with the measurement at a 2000-m distance from the electrical

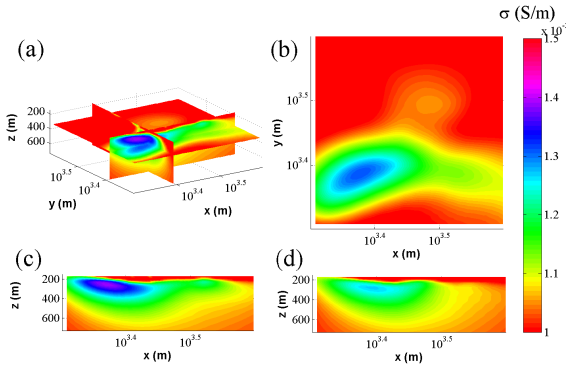

Fig. 9. Reconstructed conductivity from the GREATEM field data for a survey area in Fig. 8. (a) 3-D slices of the inverted result. (b) Horizontal slice for the survey area at $z = 300$ m depth. (c) Vertical slice through the flight C's location. (d) Vertical slice through the flight D's location.

source and at about 125-m receiver height. There are five flight lines (A–E) almost perpendicular to the line source from north to south in the survey area with the 200-m space. Although each flight line is at the length of 3 km, the field data within ∼2 km of the line source are used to reconstruct conductivity, because the data collected farther from the source have a lower SNR. The forward and inverse computation is executed at six equally sampled frequencies from 25 to 50 Hz. The scattered magnetic fields are extracted from the measured data by the method introduced in Section III-C.

In the inversion, we use a 3-D half-space as the initial model. Since there are enough drilling data from those mines, we can estimate the background conductivity of the underground region as 0.001 S/m. The computation domain is in the depth from 200 to 800 m and covers a 2000 m × 2000 m × 600 m cubic block under the survey area. It is divided into $50 \times 50 \times 15 = 37\,500$ cells. The BCGS-FFT-BIM takes 36 iterations to converge and consumes 2.83 h on the same cluster computer used in synthetic data reconstruction. Fig. 9(a) shows the 3-D reconstructed conductivity under the survey area. It is clear that the reconstructed conductivity shows more information for the subsurface structure close to the line source. Fig. 9(b) shows the plan view of reconstructed conductivity at the depth of 300 m, which reveals that the 3-D inversion result shows the continuous conductivity distribution by this survey. Fig. 9(c) and (d) shows the vertical profiles of the reconstructed conductivity along the flight lines C and D, respectively. A relatively high-conductivity anomaly is present at the depth of 200∼400 m. The maximum depth of investigation in the reconstruction is about 700 m, and the depth of investigation decreases as the distance between the helicopter and the line source increases. Although the instruments used in this GREATEM survey are prototypes and the civil activities surrounding the mineral area cause a lot of noise, the location of the high-conductivity anomaly (low resistivity region) is roughly consistent with the Controlled Source Audio-Frequency MagnetoTellurics (CSAMT) measured result provided by the Chinese Academy of Sciences, which is validated by some geological drilling data in this area. It shows that there exits an iron ore area from the depth of 150–400 m under the granite layer.

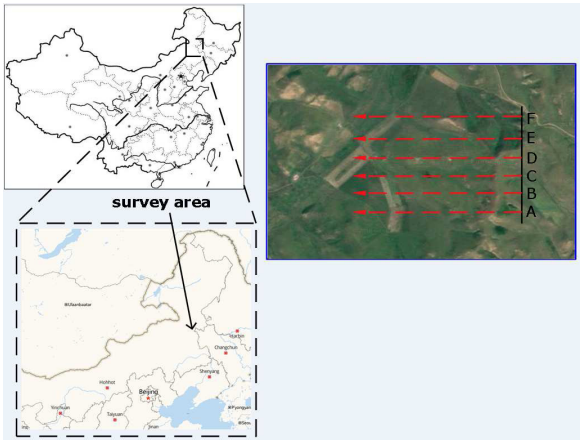

Fig. 10. Location and geometry for the GREATEM experimental survey conducted in Inner Mongolia, China. The solid line indicates the transmitter cable (electrical line source), which is placed from the north to south with the length of 1.7 km. The dashed lines (A–F) are the flight lines.

In August 2016, the same GREATEM system was used to survey the area in Inner Mongolia, China. Different from the last survey in Shandong, the experiments are performed in the grassland. Geological drilling data are very limited. The survey's scheme is shown in Fig. 10. The electric line source is placed from the north to the south. The source current moment is decreased to 9 A × 1770 m with the measurement at a 2500-m distance from the electrical source and at about 80-m receiver height. The six flight lines (A–F) are almost perpendicular to the line source from the east to west in the survey area with the 200-m space. Although each flight line is at the length of 2.5 km, the field data within ∼1.2 km of the line source are used to reconstruct conductivity due to low SNR of the data collected farther away. The forward and inverse computation is also executed at six equally sampled frequencies from 25 to 50 Hz. The data processing steps are the same as the last GREATEM experiment in Shandong.

Since there are a few geological drilling data in this survey, we have to guess different values of the background conductivity from 0.001 to 0.01 S/m to calculate the incident magnetic field as the input of the 3-D half-space model. The data misfit in the inversion is smallest when the background conductivity of the underground region is set to be 0.005 S/m. Therefore, we only show the inversion results for the background conductivity of 0.005 S/m in the following. The computation domain in this case is in the depth from 80 to 720 m and covers a 1600 m × 1600 m × 640 m cubic block under the survey area. It is divided into $50 \times 50 \times 20 = 50\,000$ cells. The BCGS-FFT-BIM takes 31 iterations to converge and consumes 3.47 h on the same cluster computer used for the last case. Fig. 11(a) shows the 3-D reconstructed conductivity under the survey area. Fig. 11(b) shows the plan view of reconstructed conductivity at the depth of 150 m. Fig. 11(c) and (d) shows the vertical profiles of the reconstructed conductivity along flight lines E and F, respectively. Two relatively high-conductivity anomalies are present at the depth of 100∼300 m. The plan view of the reconstructed result shows that there are two anomalies from the east to the west in this survey.

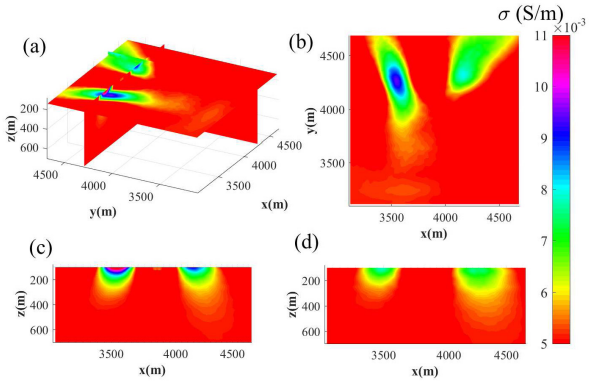

Fig. 11. Reconstructed conductivity from the GREATEM field data for a survey area in Fig. 10. (a) 3-D slices of the inverted result. (b) Horizontal slice for the survey area at $z = 150$ m depth. (c) Vertical slice through the flight line E's location. (d) Vertical slice through the flight line F's location.

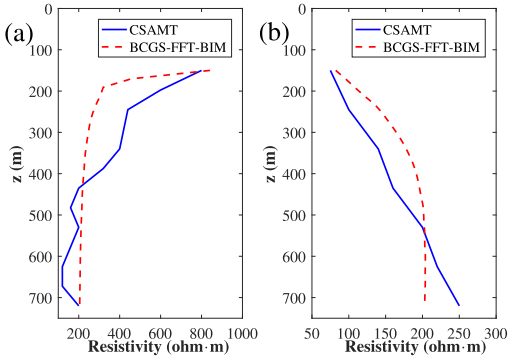

Fig. 12. 1-D transect comparisons of results at flight line F from CSAMT and BCGS-FFT-BIM. (a) Location is at $x = 3800$ m in Fig. 11(d). (b) Location is at $x = 4200$ m in Fig. 11(d).

Although the geological drilling data are limited in this area, there is a mine drilling performed near flight line F. We compare the 3-D reconstructed profiles by the BIM algorithm and the drilling data and find that the location of the anomaly, which is from 4000 to 4500 m in the x-direction, is consistent with the drilling data. Moreover, the reconstructed conductivity of this anomaly is about 0.012 S/m, which is also consistent with the drilling data. The drilling data are proprietary for mining industry cooperation. Thus, we just show the comparisons of 1-D transects between the BCGS-FFT-BIM results and the CSAMT results, which are validated by the drilling data. From Fig. 12, we can clearly see that the reconstructed resistivity of BCGS-FFT-BIM fits the data of CSAMT well with the increase of depth. The reconstructed results of this area show a promising application of our proposed method for 3-D interpretation of GREATEM data.

VI. Conclusion

In this paper, a GREATEM system designed recently is reported and the data processing technique is discussed. For the first time, the frequency-domain 3-D interpretation of the GREATEM data is performed by using BCGS-FFT with BIM. The EFIE is formulated in the low-frequency regime for the GREATEM forward scattering model. The fast solver BCGS-FFT is adopted to solve the discretized EFIE. The nonlinear inverse problem is solved by the BIM. In order to validate the proposed method, we conduct a numerical experiment first. The result shows that the 3-D multifrequency inversion algorithm is feasible for the reconstruction of the underground conductivity distribution in the GREATEM measurement with low computation and consumption.

The reconstructed results of experimental data from two campaigns show that the GREATEM survey can recover the deep conductivity structures by using a grounded line source and the 3-D BCGS-FFT-BIM algorithm. The reconstructed underground conductivity distribution from our full-wave inversion is roughly consistent with the drilling data. This means that the proposed 3-D algorithm in this paper is feasible for the interpretation of GREATEM data measured in geophysical engineering applications.

Finally, we want to emphasize two points. First, although the conductivity distribution reconstructed in this paper is based on the half-space initial model, more underground layers can be directly included in our model if the deep well logging data are available. Second, the compressive sampling theory has been combined with an inversion algorithm to improve the reconstruction results and reduce the data requirement in the Born approximation in recent years [33]–[35]. This method can potentially improve the inversion result resolution of GREATEM data. However, both of them will be left as the future research work.

References

[1] P. Elliott, "The principles and practice of FLAIRTEM," *Explor. Geophys.*, vol. 29, nos. 1–2, pp. 58–60, 1998.
[2] J. E. Dickinson, D. R. Pool, R. W. Groom, and L. J. Davis, "Inference of lithologic distributions in an alluvial aquifer using airborne transient electromagnetic surveys," *Geophysics*, vol. 75, no. 4, pp. WA149–WA161, 2010.
[3] H. Ito *et al.*, "Further investigations of underground resistivity structures in coastal areas using grounded-source airborne electromagnetics," *Earth, Planets Space*, vol. 63, no. 8, pp. e9–e12, 2011.
[4] R. S. Smith, A. P. Annan, and P. D. McGowan, "A comparison of data from airborne, semi-airborne, and ground electromagnetic systems," *Geophysics*, vol. 66, no. 5, pp. 1379–1385, 2001.
[5] T. Mogi, Y. Tanaka, K. Kusunoki, T. Morikawa, and N. Jomori, "Development of grounded electrical source airborne transient EM (GREATEM)," *Explor. Geophys.*, vol. 29, nos. 1–2, pp. 61–64, 1998.
[6] S. A. Allah *et al.*, "Three-dimensional resistivity characterization of a coastal area: Application of grounded electrical-source airborne transient electromagnetic (GREATEM) survey data from Kujukuri beach, Japan," *J. Appl. Geophys.*, vol. 99, no. 3, pp. 1–11, 2013.
[7] H. Ito, H. Kaieda, T. Mogi, A. Jomori, and Y. Yuuki, "Grounded electrical-source airborne transient electromagnetics (GREATEM) survey of Aso Volcano, Japan," *Explor. Geophys.*, vol. 45, no. 1, pp. 43–48, 2014.
[8] T. Mogi *et al.*, "Grounded electrical-source airborne transient electromagnetic (GREATEM) survey of Mount Bandai, North-Eastern Japan," *Explor. Geophys.*, vol. 40, no. 1, pp. 1–7, 2009.
[9] C.-C. Yin, X.-Y. Ren, Y.-H. Liu, Y.-F. Qi, C.-K. Qiu, and J. Cai, "Review on airborne electromagnetic inverse theory and applications," *Geophysics*, vol. 80, no. 4, pp. W17–W31, 2015.
[10] T. Wang, M. Oristaglio, A. Tripp, and G. Hohmann, "Inversion of diffusive transient electromagnetic data by a conjugate-gradient method," *Radio Sci.*, vol. 29, no. 4, pp. 1143–1156, 1994.
[11] E. Haber, D. W. Oldenburg, and R. Shekhtman, "Inversion of time domain three-dimensional electromagnetic data," *Geophys. J. Int.*, vol. 171, no. 2, pp. 550–564, 2007.
[12] F. Sugeng, "Modeling the 3D TDEM response using the 3D full-domain finite-element method based on the hexahedral edge-element technique," *Explor. Geophys.*, vol. 29, nos. 3–4, pp. 615–619, 1998.
[13] G. A. Wilson, A. P. Raiche, and F. Sugeng, "2.5D inversion of airborne electromagnetic data," *Explor. Geophys.*, vol. 37, no. 4, pp. 363–371, 2006.

[14] A. Abubakar, P. M. Van Den Berg, and T. M. Habashy, "An integral equation approach for 2.5-dimensional forward and inverse electromagnetic scattering," *Geophys. J. Int. Banner*, vol. 165, no. 3, pp. 744–762, 2006.
[15] L. H. Cox, G. A. Wilson, and M. S. Zhdanov, "3D inversion of airborne electromagnetic data," *Explor. Geophys.*, vol. 77, no. 4, pp. WB59–WB69, 2012.
[16] S. A. Allah *et al.*, "Three-dimensional resistivity modelling of grounded electrical-source airborne transient electromagnetic (GREATEM) survey data from the Nojima Fault, Awaji Island, South-East Japan," *Explor. Geophys.*, vol. 45, no. 1, pp. 49–61, 2014.
[17] B. Liang *et al.*, "A new inversion method based on distorted born iterative method for grounded electrical source airborne transient electromagnetics," *IEEE Trans. Geosci. Remote Sens.*, vol. 56, no. 2, pp. 877–887, Feb. 2018.
[18] M. R. Hestenes and E. Stiefel, "Methods of conjugate gradients for solving linear systems," *J. Res. Nat. Bur. Standards*, vol. 49, no. 6, pp. 409–436, Dec. 1952.
[19] T. K. Sarkar, "On the application of the generalized biconjugate gradient method," *J. Electromagn. Waves Appl.*, vol. 1, no. 3, pp. 223–242, 1987.
[20] H. A. van der Vorst, "Bi-CGSTAB: A fast and smoothly converging variant of Bi-CG for the solution of nonsymmetric linear systems," *SIAM J. Sci. Stat. Comput.*, vol. 13, no. 2, pp. 631–644, 1992.
[21] X. Millard and Q. H. Liu, "A fast volume integral equation solver for electromagnetic scattering from large inhomogeneous objects in planarly layered media," *IEEE Trans. Antennas Propag.*, vol. 51, no. 9, pp. 2393–2401, Sep. 2003.
[22] P. M. van den Berg and R. E. Kleinman, "A contrast source inversion method," *Inverse Problems*, vol. 13, no. 6, p. 1607, Dec. 1997.
[23] Y. M. Wang and W. C. Chew, "An iterative solution of the two-dimensional electromagnetic inverse scattering problem," *Int. J. Imag. Syst. Technol.*, vol. 1, no. 1, pp. 100–108, 1989.
[24] W. C. Chew and Y. M. Wang, "Reconstruction of two-dimensional permittivity distribution using the distorted Born iterative method," *IEEE Trans. Med. Imag.*, vol. 9, no. 2, pp. 218–225, Jun. 1990.
[25] C. Yin and D. C. Fraser, "Attitude corrections of helicopter EM data using a superposed dipole model," *Geophysics*, vol. 69, no. 2, pp. 431–439, 2004.
[26] K. A. Michalski and J. R. Mosig, "Multilayered media Green's functions in integral equation formulations," *IEEE Trans. Antennas Propag.*, vol. 45, no. 3, pp. 508–519, Mar. 1997.
[27] P. E. Wannamaker, G. W. Hohmann, and W. A. SanFilipo, "Electromagnetic modeling of three-dimensional bodies in layered earths using integral equations," *Geophysics*, vol. 49, no. 1, pp. 60–74, 1984.
[28] X. Millard and Q. H. Liu, "Simulation of near-surface detection of objects in layered media by the BCGS-FFT method," *IEEE Trans. Geosci. Remote Sens.*, vol. 42, no. 2, pp. 327–334, Feb. 2004.
[29] W. Zhang and Q. H. Liu, "Three-dimensional scattering and inverse scattering from objects with simultaneous permittivity and permeability contrasts," *IEEE Trans. Geosci. Remote Sens.*, vol. 53, no. 1, pp. 429–439, Jan. 2015.
[30] Z. Yu, J. Zhou, Y. Fang, Y. Hu, and Q. H. Liu, "Through-casing hydraulic fracture evaluation by induction logging II: The inversion algorithm and experimental validations," *IEEE Trans. Geosci. Remote Sens.*, vol. 55, no. 2, pp. 1189–1198, Feb. 2017.
[31] Q. H. Liu, "An FDTD algorithm with perfectly matched layers for conductive media," *Microw. Opt. Technol. Lett.*, vol. 14, no. 2, pp. 134–137, 1997.
[32] M. Bevacqua, L. Crocco, L. Di Donato, T. Isernia, and R. Palmeri, "Exploiting sparsity and field conditioning in subsurface microwave imaging of nonweak buried targets," *Radio Sci.*, vol. 51, no. 4, pp. 301–310, 2016.
[33] M. Ambrosanio and V. Pascazio, "Three-dimensional subsurface imaging of weak scatterers by using compressive sampling," in *Proc. IEEE Int. Geosci. Remote Sens. Symp.*, Jul. 2015, pp. 1056–1059.
[34] M. Ambrosanio, P. Kosmasy, and V. Pascazio, "An adaptive multi-threshold iterative shrinkage algorithm for microwave imaging applications," in *Proc. 10th Eur. Conf. Antennas Propag.*, Apr. 2016, pp. 1–3.
[35] G. Oliveri, N. Anselmi, and A. Massa, "Compressive sensing imaging of non-sparse 2D scatterers by a total-variation approach within the Born approximation," *IEEE Trans. Antennas Propag.*, vol. 62, no. 10, pp. 5157–5170, Oct. 2014.

Chen Qiu received the B.S. degree in electronic information science and technology and the M.A. degree in theoretical physics from Xiamen University, Xiamen, China, in 2010 and 2013, respectively, where he is currently pursuing the Ph.D. degree.

His research interests include fast 3-D electromagnetic forward and inverse scattering algorithm and their applications in airborne transient electromagnetics and ground penetrating radar.

Bingyang Liang received the B.E. degree in communication engineering from PLA Information Engineering University, Zhengzhou, China, in 2011, and the M.S. degree in electronics and communication engineering from Xiamen University, Xiamen, China, in 2014, where he is currently pursuing the Ph.D. degree.

His research interests include the forward and inversion method of electromagnetics and acoustics and their applications in airborne transient electromagnetics and photoacoustic tomography.

Feng Han (M'17) received the B.S. degree in electronic science from Beijing Normal University, Beijing, China, in 2003, the M.S. degree in geophysics from Peking University, Beijing, in 2006, and the Ph.D. degree in electrical engineering from Duke University, Durham, NC, USA, in 2011.

He is currently an Assistant Professor with the Institute of Electromagnetics and Acoustics, Xiamen University, Xiamen, China. His research interests include ionosphere remote sensing by radio atmospherics, electromagnetic full-wave inversion by integral equations, reverse time migration image, and the design of an electromagnetic detection system.

Hai Liu (S'11–M'13) received the B.E. and M.E. degrees in civil engineering from Tongji University, Shanghai, China, in 2007 and 2009, respectively, and the Ph.D. degree in environmental studies from Tohoku University, Sendai, Japan, in 2013.

From 2013 to 2014, he was with the Center for Northeast Asian Studies, Tohoku University, as a Research Fellow. From 2014 to 2017, he was an Assistant Professor with the Institute of Electromagnetics and Acoustics, Xiamen University, Xiamen, China. He is currently an Associate Professor with the School of Civil Engineering, Guangzhou University, Guangzhou, China. His research interests include the development of ground-penetrating radar systems and algorithms for a wide variety of applications, such as nondestructive testing in civil engineering, environmental monitoring, archeological investigation, and lunar exploration.

Dr. Liu received the Young Researcher Award from the 14th International Conference on Ground Penetrating Radar in 2012 and the Excellent Paper Award from the IET International Radar Conference in 2013.

Chunhui Zhu received the Ph.D. degree in control science and engineering from the Harbin Institute of Technology, Harbin, China, in 2012.

From 2009 to 2011, she was a Visiting Student with the Electrical Engineering Department, Duke University, Durham, NC, USA. Since 2013, she has been with Xiamen University, Xiamen, China, where she is currently an Assistant Professor with the Department of Electronic Science. Her research interests include fast algorithms for computational electromagnetics and their applications in engineering.

Na Liu (M'18) received the Ph.D. degree in computational mathematics from the University of Chinese Academy of Sciences, Beijing, China, in 2013.

From 2012 to 2013, she was a Visiting Student with the Department of Electrical and Computer Engineering, Duke University, Durham, NC, USA. From 2013 to 2017, she held a post-doctoral position at Xiamen University, Xiamen, China, where she is currently an Associate Professor with the Institute of Electromagnetics and Acoustics. Her research interests include computational electromagnetics, especially the fast and efficient methods for complex media and their applications in cavities and optical waveguide problems.

Fubo Liu, photograph and biography not available at the time of publication.

Guangyou Fang received the B.S. degree in electrical engineering from Hunan University, Changsha, China, in 1984, and the M.S. and Ph.D. degrees in electrical engineering from Xi'an Jiaotong University, Xi'an, China, in 1990 and 1996, respectively.

From 1990 to 1999, he was an Engineer, an Associate Professor, and a Professor with the China Research Institute of Radio Wave Propagation. From 2000 to 2001, he was a Visiting Scholar with the University of Trieste, Trieste, Italy, and the International Center for Science and High Technology, Trieste. From 2001 to 2003, he was a special foreign Research Fellow of the Japan Society for Promotion of Science, working with the Prof. M. Sato, with Tohoku University, Sendai, Japan. He was a PI of CE-3 lunar penetrating radar. Since 2004, he has been a Professor with the Institute of Electronics of the Chinese Academy of Sciences (IECAS), Beijing, China, the Director of the Key Laboratory of Electromagnetic Radiation and Sensing Technology, CAS, and the Deputy Director of IECAS since 2013. He has published over 300 papers in refereed journals and conference proceedings. His research interests include electromagnetic field theory, ultrawideband radar, ground-penetrating radar, lunar and mars exploration radar, geophysical electromagnetic exploration technology, and terehertz imaging.

Qing Huo Liu (S'88–M'89–SM'94–F'05) received the B.S. and M.S. degrees in physics from Xiamen University, Xiamen, China, in 1983 and 1986, respectively, and the Ph.D. degree in electrical engineering from the University of Illinois at Urbana–Champaign, Champaign, IL, USA, in 1989.

From 1986 to 1988, he was a Research Assistant with the Electromagnetics Laboratory, University of Illinois at Urbana–Champaign, where he was a Post-Doctoral Research Associate from 1989 to 1990. He was a Research Scientist and the Program Leader with Schlumberger-Doll Research, Ridgefield, CT, USA, from 1990 to 1995. From 1996 to 1999, he was an Associate Professor with New Mexico State University, Las Cruces, NM, USA. Since 1999, he has been with Duke University, Durham, NC, USA, where he is currently a Professor of electrical and computer engineering. He has authored over 400 papers in refereed journals and 500 papers in conference proceedings. His research interests include computational electromagnetics and acoustics, inverse problems, and their applications in nanophotonics, geophysics, biomedical imaging, and electronic packaging.

Dr. Liu is a fellow of the Acoustical Society of America, the Electromagnetics Academy, and the Optical Society of America. He received the 1996 Presidential Early Career Award for Scientists and Engineers from the White House, the 1996 Early Career Research Award from the Environmental Protection Agency, the 1997 CAREER Award from the National Science Foundation, and the 2017 ACES Technical Achievement Award. He served as a Guest Editor for the PROCEEDINGS OF THE IEEE. Since 2015, he has been the Founding Editor-in-Chief of the new IEEE JOURNAL ON MULTISCALE AND MULTIPHYSICS COMPUTATIONAL TECHNIQUES. He currently serves as the Deputy Editor-in-Chief for the *Progress in Electromagnetics Research*, an Associate Editor for the IEEE TRANSACTIONS ON GEOSCIENCE AND REMOTE SENSING, and an Editor for the *Journal of Computational Acoustics*. He served as an IEEE Antennas and Propagation Society Distinguished Lecturer from 2014 to 2016.